BMC Plant Biology

RESEARCH

Open Access

Comprehensive proteomic profiling of *Cucumber mosaic virus* infection: identifying key proteins and pathways involved in resistance and susceptibility in melon

Núria Real[1], Antoni Garcia-Molina[1], Sara Christina Stolze[2], Anne Harzen[2], Hirofumi Nakagami[2] and Ana Montserrat Martín-Hernández[1,3*]

Abstract

Background Melon (*Cucumis melo L.*) is the model species of the *Cucurbitaceae* family and an important crop. However, its yield is primarily affected by viruses. *Cucumber mosaic virus* (CMV) is particularly significant due to its broad host range, capable of infecting over 100 plant families. Resistance to CMV in the melon accession Songwhan Charmi (SC) is controlled by the recessive gene *cmv1*, which encodes the *Vacuolar Protein Sorting 41*, involved in vesicle transport to the vacuole. *cmv1* restricts the virus to the bundle sheath cells and impedes viral access to the phloem, preventing a systemic infection. This phenotype depends on the viral movement protein (MP). However, little is known about the broader cellular changes that CMV triggers in melon or the specific biological responses that facilitate or restrict the virus entry into the phloem in susceptible and resistant varieties.

Result We profiled the proteomes of CMV-resistant or susceptible melon genotypes inoculated with CMV-LS or FNY strains. Analysis of co-abundance networks revealed the rewiring of central biological pathways during different stages of CMV infection. Upon inoculation, resistant varieties do not trigger any signalling event to the new leaves. Local infection triggers a general depletion in proteins related to translation, photosynthesis and intracellular transport, whereas only in resistant varieties CMV triggers an increase in lipid modification and phloem proteins. During the systemic infection of susceptible melon plants, there is a strong increase in proteins associated with stress responses, such as those involved in the ER-associated degradation (ERAD) and phenylpropanoid pathways, along with a decrease in translation and photosynthesis. Key hub proteins have been identified in these processes.

Conclusions This study is the first comprehensive high-throughput proteomic analysis of CMV-infected melon plants, providing a novel and detailed understanding of the proteomic changes associated with CMV infection, highlighting the differential responses between resistant and susceptible genotypes and identifying key proteins that could be potential targets for future research and CMV management strategies.

Keywords CMV, Proteome, Cucumis melo, Resistance

*Correspondence:
Ana Montserrat Martín-Hernández
montse.martin@irta.es
Full list of author information is available at the end of the article

Introduction

Viruses are obligate intracellular parasites that encode only a few proteins, although some of them carry out several functions [1]. Consequently, viruses need to subvert the host machinery to redirect the cell metabolism to favour viral replication and complete their life cycle. Thus, most factors involved in viral infection are host proteins, which are used by the virus in different steps of the viral cycle in a dynamic manner [2]. Shortly after viral infection, plant viruses manipulate the host physiology to provide energy resources to favour their replication and protein synthesis and divert these resources to cell locations where this replication takes place [3]. At later stages, the plant responds triggering defence responses by increasing reactive oxygen species (ROS) and carbohydrate metabolism and respiration to reduce the damage caused and restore as much as possible the normal cell functions, while reducing photosynthesis [4, 5]. These host immune responses cause symptomatic manifestations such as chlorotic lesions or spots, ringspots and necrotic lesions in infected cells [6].

At a molecular level, physiological processes affected by viral infection include (i) carbohydrate and amino acid biosynthesis that might be upregulated or downregulated depending on the virus or the proteins involved in this process [7], (ii) plant hormone signalling, causing changes that are related to developmental abnormalities such as stunting and leaf curling [8], (iii) photosynthesis and photorespiration, which might be a direct effect of the viruses or a result of infection due to chloroplast damage [9], (iv) synthesis of pathogen defence proteins, such as pathogenesis-related proteins, chitinases, peroxidases, among others [10], as well as (v) stress responses such as the production of ROS that are accumulated in response to the oxidative stress caused by the infection and directly participate in cell death pathways [11].

CMV has the highest host range within plant viruses, being able to infect more than 1,200 plant species distributed throughout the globe, colonizing both temperate and tropical ecosystems [12, 13]. Its ability to adapt to new environments and hosts has resulted in the emergence of numerous strains, which are divided in two main subgroups (SG), based on their sequence homology, SG I and SG II. CMV symptoms range from mosaic and distortion of the leaves to fruit lesions, including chlorosis, leaf deformation and dwarfism depending on the host and viral strain [14]. Resistance to CMV is often oligogenic and quantitative [15, 16]. In *Cucumis melo*, the model species of the Cucurbitaceae family, few sources of resistance have been found, most of them oligogenic and recessive [17–21]. Resistance found in the accession PI 161375, cultivar Songwhan Charmi (SC) is also quantitative, composed of one major gene, *cmv1*, providing resistance to CMV strains belonging to subgroup II and at least two QTL that, in coordination with *cmv1*, provide resistance to subgroup I strains [22]. Among the numerous genetic resources already developed [23], a collection of near-isogenic lines (NILs) generated from a cross between the CMV-susceptible Spanish cultivar Piel de Sapo (PS) and the CMV-resistant cultivar SC [24] allowed to unveil the genetics of the resistance to CMV. The NIL SC 12–1–99, which carries a *cmv1* introgression from the resistant melon SC in the genetic background of the susceptible melon PS, is resistant to CMV-LS (from SG II) and susceptible to CMV-FNY (from SG I) [25]. *cmv1* allows replication and cell-to-cell movement of CMV-LS, but it impedes reaching the phloem by restricting the virus at the bundle sheath cells, thus preventing a systemic infection. On the other hand, *cmv1* is unable to stop phloem invasion of CMV-FNY (SG I), allowing a systemic infection [26]. This difference depends on the movement protein (MP) of the infecting strain since a recombinant CMV-LS virus carrying FNY MP can develop a systemic infection in the *cmv1*-carrying SC-12–1–99 melon line [27].

cmv1 encodes a Vacuolar Protein Sorting 41 (CmVPS41) [28], a protein involved in the intracellular movement of cargo proteins from the late Golgi, via late endosomes or vesicles, to the vacuole as part of the "homotypic fusion and vacuole protein sorting" (HOPS) complex [29, 30]. In the susceptible melon plant, VPS41 forms transvacuolar strands that are absent in the resistant plant. These transvacuolar strands are formed by late endosomes and would be part of the mechanism by which CMV can move intracellularly inside the BS cells to reach the plasmodesmata (PDs) facing the phloem [31]. However, a more precise elucidation of the CMV infection/resistance mechanisms in melon requires a broader knowledge of proteins involved in the infection.

Transcriptome approaches have been widely used to study biotic stress responses of plants [32]. However, mRNA changes might not always correlate with changes at the protein level. There are only two proteomic studies in melon, both addressing exclusively the analysis of phloem proteome, either upon *Melon necrotic spot virus* (MNSV) infection or upon CMV infection. Both use 2D gel electrophoresis coupled to MS technique, which limits the number of proteins captured [33, 34]. To better understand the melon response to CMV, here we have used liquid chromatography-tandem mass spectrometry (LC–MS/MS) to increase proteome coverage and have generated protein co-abundance networks for either local or systemic infection to understand the molecular pathways modified upon viral infection. We have compared the proteome changes in the susceptible PS plant with those occurring in the resistant SC or the NIL 12–1–99,

resistant to CMV-LS systemic infection and susceptible to CMV-FNY. Our results contribute valuable insights into the molecular pathways involved in CMV infection in melon.

Material and methods

Growth of plants, viral inoculations and sample collection

The melon genotypes used were the Spanish cultivar Piel de Sapo (PS), susceptible to CMV, the Korean accession PI 161375, cultivar "Songwhan Charmi" (SC), resistant to CMV, provided by Semillas Fitó SA (Barcelona, Spain) and "La Mayora" research station (Málaga, Spain). The Near Isogenic Line (NIL) SC12-1–99, carrying a short introgression from SC in the linkage group XII, which contains the gene *cmv1* was reported previously from our laboratory (25). Melon seeds were treated with 2.5 g/L Merpan (ADAMA Essentials, Spain) for 5 min, rinsed, and soaked in water overnight. Seeds were pre-germinated for 3 days at 28 ºC with 12 h light (100 µmols/m^2 s^1) / 12 h dark cycles. The seedlings were planted and grown in a fitotron chamber (Fitotronic Version2, Inkoa, Spain) under long-day conditions (22 ºC, 16 h light; 18 ºC, 8 h dark).

CMV strains LS and FNY were propagated in zucchini squash (*Cucurbita pepo L.*) Chapin F1 (Semillas Fitó SA, Barcelona, Spain) in a SANYO MLR-350H growth chamber under the same light/dark conditions. Viral sap from infected zucchini squash was prepared by grinding new leaves in 0.2% diethyl dithiocarbamate (DIECA) buffer with active carbon. Melon cotyledons (7–10 days old) were rub-inoculated with viral sap. Samples were collected from the same melon plants: cotyledons at 4 days-post-infection (dpi) (local infection) and new leaves at 15 dpi (systemic infection). Four biologically independent replicates of local and systemic infections or the corresponding mocks were harvested for each plant-virus combination.

Protein extraction, fractionation and digestion

Frozen melon leaves or cotyledons were ground with liquid nitrogen. 200 µL urea/DTT extraction buffer (8M urea, 5 mM DTT, 100 mM Tris, pH 8.5, Carl Roth, Karlsruhe, Germany) with protease inhibitor cocktail 2 and 3 (20 µL/mL, Sigma, St. Louis, USA) was added to 50 µL of the plant material, mixed, and incubated for 30 min at room temperature (RT). The supernatant was transferred after centrifugation (10 min, 10,000 × g), and this was repeated until no pellet remained. Protein concentration was determined using the Pierce 660 nm protein assay (Thermo Fisher Scientific, Waltham, USA).

For digestion, samples were alkylated with 14 mM chloroacetamide (Sigma, St. Louis, USA) for 30 min at RT in the dark, then diluted with 100 mM Tris, pH 8.5, 1 mM $CaCl_2$. 0.5 µg Lys-C (WAKO, Neuss, Germany) was added and incubated for 4 h at 37 °C. Samples were further digested overnight with 0.5 µg trypsin. After acidification with 20 µL 50% TFA, samples were split for BoxCar and library samples. For library samples, SCX fractionation was performed using StageTips with an ammonium acetate gradient. For BoxCar analysis, peptides were desalted with C18 Empore disk membranes.

Liquid Chromatography with tandem Mass Spectrometry (LC–MS/MS)

Library samples were analyzed using an EASY-nLC 1200 coupled to a Q Exactive Plus mass spectrometer (Thermo Fisher Scientific, Waltham, USA). Peptides were separated on a 16 cm frit-less silica emitter (New Objective, 75 µm inner diameter) packed in-house with reversed-phase ReproSil-Pur C18 AQ 1.9 µm resin (Dr. Maisch) and eluted over 115 min with a segmented linear gradient (5–95% solvent B). MS spectra were acquired in data-dependent acquisition mode with a TOP15 method. MS spectra were acquired in the Orbitrap analyzer with a mass range of 300–1750 m/z at a resolution of 70,000 FWHM, and precursors were selected with an isolation window of 1.3 m/z. Higher-energy C-trap dissociation (HCD) fragmentation was performed at a normalized collision energy of 25. MS spectra were acquired with a target value of 10^5 ions at a resolution of 17,500 FWHM and a fixed first mass of m/z 100. Peptides with a charge of + 1, greater than 6, or with an unassigned charge state were excluded from fragmentation for MS. Dynamic exclusion for 30 s prevented repeated selection of precursors.

For BoxCar samples, the same equipment was used with MaxQuant Live for acquisition. One full MS scan was followed by two BoxCar scans. The acquisition consisted of one full MS scan with a mass range of 300–1650 m/z at a resolution of 140,000 FWHM. This was followed by two BoxCar scans, each consisting of 10 boxes with 1 Da overlap and a scan range from 400–1200 m/z. The most abundant ions were selected for HCD fragmentation at a normalized collision energy of 27. Precursors were selected with an isolation window of 1.4 m/z. MS/MS spectra were acquired with a target value of 10^5 ions at a resolution of 17,500 FWHM and a fixed first mass of m/z 50. Peptides with a charge of + 1, greater than 5, or with an unassigned charge state were excluded from fragmentation for MS. Dynamic exclusion for 30 s prevented repeated selection of precursors.

Proteome analysis

Raw data were processed using MaxQuant (version 1.6.3.4) with label-free quantification (LFQ) [35]. MS/MS spectra were searched with the Andromeda search

engine against the *C. melo* version CM4.0 [https://www.melonomics.net, [36]], including CMV movement proteins and common contaminants. Trypsin specificity was required, allowing for a maximum of two missed cleavages. Carbamidomethylation of cysteine residues was set as fixed, while oxidation of methionine and protein N-terminal acetylation were set as variable modifications. The match between runs option was enabled. Peptide-spectrum-matches and proteins were retained if they were below a 1% false discovery rate (FDR).

Statistical analysis of MaxLFQ values was carried out using Perseus (version 1.5.8.5). Quantified proteins were filtered for reverse hits and hits "only identified by site," and MaxLFQ values were log2 transformed. Next, the data was separated for a mixed imputation processing: hits were filtered for 3 valid values in one of the conditions. Then, the data was separated into two sets: one set containing mostly missing at random (MAR) hits and the other set containing mostly missing not at random (MNAR) hits by filtering the data for 1 valid hit in each group and splitting the resulting matrices [37]. The resulting matrix with at least 1 valid hit in each group was the MAR dataset, the matrix with the hits filtered out was the MNAR dataset. The missing values of each dataset were then imputed using different options of the "imputeLCMD" R package [38] integrated into Perseus: the missing values from the MAR dataset were imputed using a nearest neighbor approach (KNN, $n=4$), the missing values from the MNAR dataset were imputed using the MinProb option (q = 0.01. tune.sigma = 1). After merging of the imputed datasets two-sample Student's t-tests for pair-wise comparisons was performed using a permutation-based FDR of 5%. The Perseus output was exported and further processed using Excel. Significant proteins were filtered by absolute $\log_2$ fold-change ≥ 1 and adjusted $P \leq 0.05$ using a permutation-based for false discovery rate.

Elaboration of heatmaps

Heatmaps with hierarchical clustering were drawn with z-score normalized protein abundances and grouped according to the Ward.D2 method using the RStudio *pheatmap* package.

Elaboration and analysis of co-abundant protein networks

Co-abundant protein networks were constructed from the imputed datasets of relative intensity abundance (MaxLFQ) of all detected proteins in LC–MS/MS. Proteome datasets were filtered to exclude proteins that did not change under any of the treatments (one-way ANOVA, $P \leq 0.05$). Then, pair-wise Pearson correlations were computed to detect significant co-abundant proteins across all treatments (adjusted $P \leq 0.05$ according to the Benjamini–Hochberg correction) to define node connectivity in each network. The Pearson correlation coefficient (r) cut-off was at the moment where the resulting network display the lowest density to preserve the main number of connections (edges) while avoiding saturation. Network properties were analysed with the RStudio *igraph* package and exported to Cytoscape, version 3.8.2 [39] for visualization and further analysis. Network communities were detected according to the fast greedy method [40]. Functional annotation of modules was based on significant enrichment (adjusted $P \leq 0.05$, Fisher's exact test with Benjamini–Hochberg correction) in Gene Ontology (GO) terms and Kyoto Encyclopaedia of Genes and Genomes (KEGG) using the RStudio *gprofiler2* package [41].

Results and discussion

Resistance to CMV-LS does not trigger any signalling from local to new tissues in the proteome of new leaves

SC and PS cultivars display antagonistic responses against CMV infection, being SC resistant and PS susceptible. However, NIL melon plants, carrying *cmv1* gene from SC, display susceptibility to CMV-FNY [27] but resistance to CMV-LS due to arrest in virus progression at the bundle sheath [26]. Viral symptoms in susceptible plants are the typical mosaic in systemic leaves [27, 42]. Since the molecular basis of such plant-virus interaction is poorly understood, we aimed to investigate the consequences of CMV infection at the protein level in resistant (SC/CMV-LS, SC/CMV-FNY and NIL/CMV-LS) and susceptible (PS/CMV-LS, PS/CMV-FNY and NIL/CMV-FNY) melon-virus combinations. To this end, inoculated cotyledons at 4 dpi and in newly developed leaves at 15 dpi were collected to monitor local and systemic proteome changes upon infection of the three melon genotypes with either CMV-FNY or CMV-LS strains. LC–MS/MS proteomic profiling provided an overall coverage of approximately 5,000 proteins from either local or systemic infections (Tables S1 and S2). To capture patterns of changes in protein abundance during local and systemic responses to CMV infections, relative intensity values of each protein were z-score normalised and used to draw heatmaps with hierarchical clustering. To get a first insight into the global strategies of melon plants to respond to CMV infection, proteome changes were clustered per genotype (SC, PS, NIL) and treatment (mock, CMV-FNY, CMV-LS). In local responses, proteomes of SC mock-inoculated and inoculated plants were certainly homogeneous and clearly separated from those of NIL and PS, although mock-inoculated PS and NIL plants could be further discriminated from their inoculated counterparts (Fig. 1A). Hence, despite important differences in proteome composition due to genotypes,

singular proteome reconfigurations among melon plants took place in response to local virus inoculation. On the other hand, systemic proteome responses for CMV-susceptible combinations (PS/CMV-FNY, PS/CMV-LS and NIL/CMV-FNY) were uniform and differentiated from CMV-resistant combinations (SC/CMV-FNY, SC/CMV-LS and NIL/CMV-LS) and mock-inoculated plants (Fig. 1A). Thus, our analysis indicates a general absence of perturbations at proteome level in new leaves of resistant plants, suggesting an absence of signalling from inoculated, virus containing, cotyledons to new leaves. Moreover, the results unveil that the resistance of the NIL against CMV-LS acquired by the introgression of *cmv1* in the PS background does not cause any pay-off in the systemic tissues (Fig. S1).

However, the molecular mechanisms determining these distinct responses to CMV-LS and FNY in the NIL remain elusive. To shed some light into the proteome changes in inoculated NIL plants depending on the virus strain, we identified differentially abundant proteins (DAPs) between plants locally or systemically infected with either CMV-FNY or LS (absolute $\log_2$ fold-change ≥ 1, adjusted $P \leq 0.05$, Student's t-test). At local level, the NIL displayed similar number of DAPs in the presence of both viruses as depicted in the volcano plots (Fig. 1B), which could suggest a similar number of cells being infected by both viruses. In systemic infections, NIL/CMV-FNY showed a substantial proteome shift (Fig. 1B), with DAPs increasing four times with respect to the local infection (Table S3) reflecting the strong infection and the exploitation of host resources in all leaf tissues. In contrast, new leaves of NIL/CMV-LS displayed no DAPs (Fig. S1), reflecting the lack of systemic infection and the absence of signalling from inoculated cotyledons that could be sensed in new leaves. To further investigate whether the DAPs in NIL/CMV-LS plants were common to those in SC/CMV-LS inoculated plants, we analysed the overlap in DAPs. As shown in the Venn diagram in Fig. 1C, 21 DAPs (8.6% from NIL, 28.4% from SC) were common in the local infection between SC/CMV-LS and NIL/ CMV-LS plants, while only one DAP was shared with PS/CMV-LS plants. This suggests that some of the events taking place in both resistant genotypes upon inoculation are partially similar (Fig. 1C). In conclusion, these findings indicate that NIL plants infected with CMV-LS resemble the resistant SC cultivar at both local and systemic infection stages. Moreover, despite the local proteomic response in cotyledons in both SC and NIL/CMV-LS inoculated plants, there are no signalling events in new leaves during the systemic infection, where no DAPs were detected.

Co-abundant proteome networks reflect the rewiring of central biological processes in melon plants under CMV infection

Networks of co-abundant proteins under local and systemic infections were constructed to provide a holistic interpretation of CMV infection based on functional annotation of communities. Briefly, proteins that did not significantly change under any of the treatments were filtered out ($P < 0.05$, one-way ANOVA). Then, pair-wise correlation of relative intensity values of proteins was computed to infer connections and accordingly determine modules of co-abundant proteins. Topologically, both local and systemic networks showed a similar scale (500 and 187 nodes), density (0.04) and modularity (0.4–05, that led to 5 and 6 communities with more than 10 proteins, respectively), but differed in shape (4,696 and 681 edges) and thus average number of neighbours (18.78 vs 7.28) (Table 1). Interestingly, most proteins in the network were exclusive in each case (70% and 84% in the systemic and local infection networks respectively), suggesting that different players are involved in each response.

Functional annotation of the protein communities revealed both shared and unique biological processes between the networks. As observed in Table 2, while both the local and systemic networks showed some enrichment in fundamental processes such as metabolism, translation, carbon fixation, or glycolysis, there were notable differences in specialized functions. For example, certain modules in the local network are enriched in some processes related to stress, such as response to toxic substances lipid, nitrogen, and sulfur metabolism,

(See figure on next page.)

Fig. 1 Melon proteome changes in response to CMV infection. **A**. Heatmaps of melon proteome responses to CMV local or systemic infection. Hierarchical clustering was performed according to the WardD2 method with Z-means of the relative intensity abundance values of each protein per treatment. SC mock: SC/mock-inoculated. SC FNY: SC/CMV-FNY-inoculated. SC LS: SC/CMV-LS-inoculated. NIL mock: NIL/mock-inoculated. PS mock: PS/mock-inoculated. NIL FNY: NIL/CMV-FNY-inoculated. NIL LS: NIL/CMV-LS-inoculated. PS FNY: PS/CMV-FNY-inoculated. PS LS: PS/CMV-LS-inoculated. Gray: mock-inoculated plants. Red: susceptible combinations. Blue: resistant combinations. **B**. Volcano plots were generated according to $\log_2$ -transformed fold-change and -$\log_{10}$ FDR values. Significantly enriched (red) and depleted (cyan) proteins in NIL/CMV-inoculated vs non-inoculated plants (local) and in NIL/CMV-FNY vs mock-inoculated plants in systemic infection (systemic). **C**. Venn diagram of the DAPs during local infection shared between NIL CMV-LS compared to SC and PS both CMV-LS inoculated (all DAPs with respect to their corresponding mock-inoculated plants). Volcano plots were generated with an absolute log2 in fold-change ≥ 1 (adjusted $P \leq 0.05$, Student's t test)

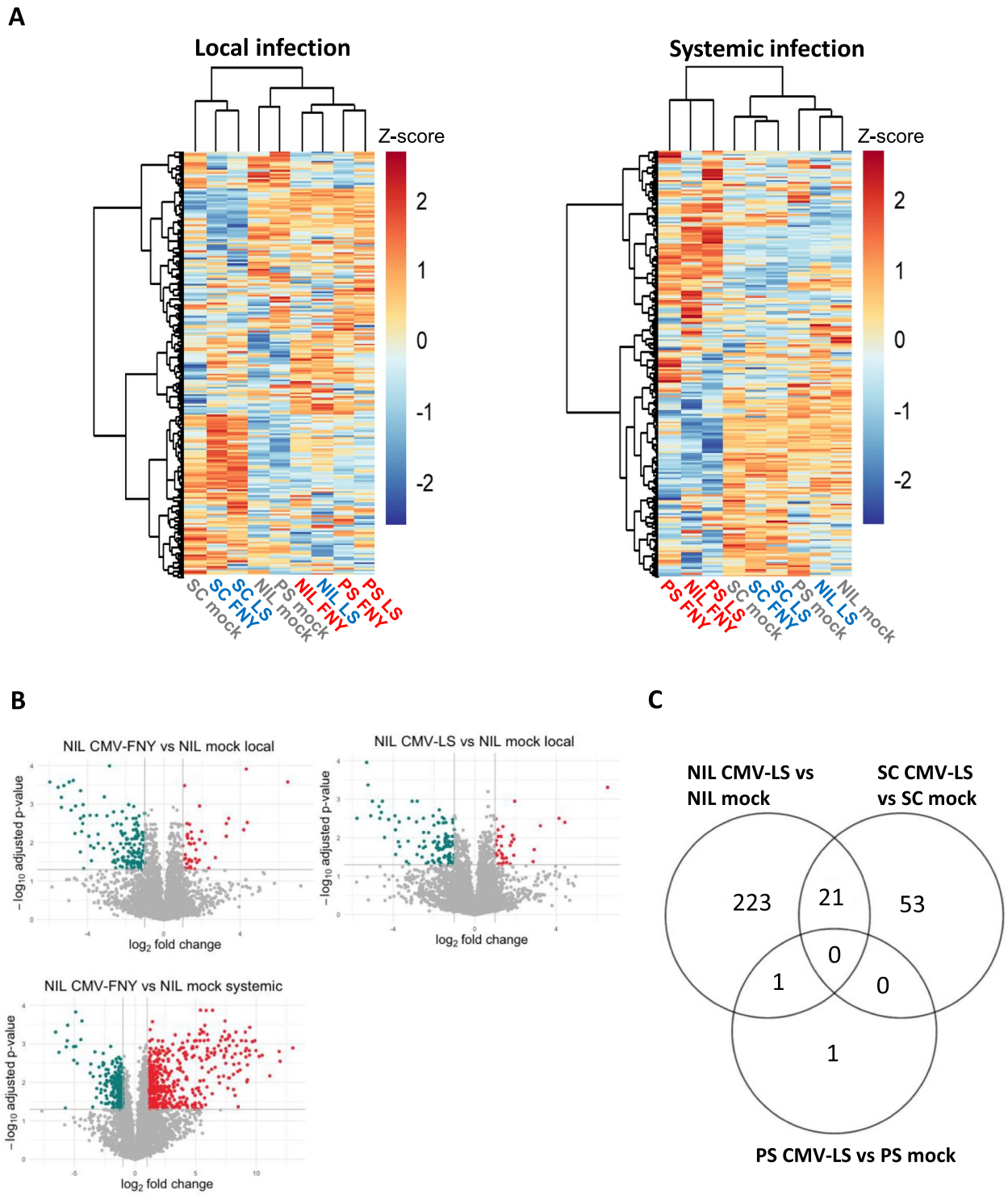

Fig. 1 (See legend on previous page.)

and even processes related to virus infection and progression such as systemic acquired resistance and phloem development, highlighting the distinct biological roles that these modules play locally. Conversely, the systemic network was enriched in secondary metabolism related to glyoxylate and dicarboxylate metabolism, as well as phenylpropanoid biosynthesis, RNA binding and protein degradation and export. This distinction underscores the

Table 1 Topological analysis of co-abundance networks of proteins

	Local network	Systemic network
Nodes	500	187
Edges	4,696	681
Average number of neighbours	18.78	7.28
Network density	0.04	0.04
Modularity	0.44	0.53
Modules	5	6

specialized functions of different modules in local versus systemic networks, emphasizing the unique biological roles that they fulfil in response to specific conditions. For the detailed results refer to Table S4. This observation points to a clear example of specialization in plant tissues, where different proteins are responsible for similar biological processes. Specialization of gene expression across different tissues in melon has been previously reported, with tissue-specific gene expression patterns observed, particularly in fruit development and ripening stages [43].

Resistant melon genotypes reconfigure proteomes during local CMV Infection by increasing the abundance of phloem proteins and lipoxygenases related to defence and systemic signalling

After functionally annotating the communities of co-abundant proteins in both networks, we used this broad biological context to map the DAPs and employed a guilty-by-association approach to better understand their functions within this broader biological framework [44]. This approach allowed to identify which biological processes are relevant in the response to CMV infection. Specifically, in each network DAPs from six pairwise comparisons were mapped within each cultivar (PS, SC and NIL) infected or not with CMV (Table S5). However, in the local network two pair-wise comparisons were excluded: PS/CMV-LS vs PS mock-inoculated plants and NIL/CMV-FNY vs NIL/CMV-LS-inoculated plants, since the respective DAPs identified (2 and 4 respectively) did not meet the stringent criteria for inclusion in the highly filtered network ($r > 0.88$), which limited the ability to assess further CMV's impact on these comparisons. In the local network, there was a generalised decrease in abundance in processes related to translation, pigment and secondary metabolite synthesis, and lipid modification (module 3 in Fig. 2A). Depletion of proteins in this module could be part of the defence surveillance that plants have evolved to face viruses, which includes among others, a general translation repression at the beginning of the infection, to counteract the viral need for the cellular translation machinery [45].

Network communities are governed by local hubs, i.e., the nodes with the highest connectivity within each community, and are informative about coordinated proteomic changes. According to this, there are two hubs decreasing in abundance in this module, a Tubulin alpha chain (MELO3C009504.2.1), which would be needed for intracellular transport of virus particles towards PDs [46] and a 50S ribosomal L3 (MELO3C022485.2.1) a ribosomal protein directly involved in translation (Fig. 2B). On the contrary, in the other modules, the mapped DAPs reveal a trend of general increase in abundance in all groups. Notably, there is no decrease in abundance in proteins in module 3 shared by the groups NIL/CMV-LS and SC/CMV and proteins exclusive to SC/CMV, which are combinations resistant to phloem entry and systemic infection, which might suggest that in the resistant combinations the amount of virus does not reach a point where the plants suffer a depletion in proteins devoted to translation, pigment and secondary metabolite synthesis, or lipid modification. Exclusive also to these combinations is the increased co-abundance in proteins of module 5 (lipid modification, photosynthesis and carbon and energy metabolism). In this module, three lipoxygenases (LOX) stand out, one of them is a PLAT (Polycystin-1, Lipoxygenase, Alpha-Toxin) domain-containing protein (MELO3C031065.2.1), present in a variety of membrane or lipid-associated proteins, which has a role in both biotic [47] and abiotic stresses [48]. LOXs modify lipid metabolism, which viruses need for their replication and transport. In the resistant combinations, CMV replication is still actively ongoing in the few cells invaded on its way to the veins [27] and therefore proteins involved in lipid metabolism would still need to be recruited. In melon LOXs 9 and 13 are induced upon wounding and fungal infection [49]. They also direct the synthesis of oxylipins, which are involved in plant defence and signalling and have been reported as positive regulators of programmed cell death during diverse viral infections [50]. LOXs also catalyze the oxygenation of polyunsaturated fatty acids, leading to the production of signalling molecules that modulate stress responses [51]. Thus, viral inoculation via wounding during the rub inoculation, as was performed in this study, could have induced the accumulation of some LOXs. Interestingly, the PLAT domain-containing protein was also co-abundant with a phloem protein 2-like A1 from module 2, which was in turn co-abundant with several proteins of the phloem, such as a 26 kDa phloem lectin, a phloem protein 2-like A4, and a Sieve elements occlusion B. Additionally, one of the lipoxygenases was co-abundant with

Table 2 Functional characterization of each module for melon local and systemic networks using a GO and KEGG enrichment (Fisher test; FDR ≤ 0.05). Enriched biological processes are orange coloured

	Local modules					Systemic modules					
Biological Process	**1**	**2**	**3**	**4**	**5**	**1**	**2**	**3**	**4**	**5**	**6**
Common biological processes											
Amino acid metabolism	■			■		■		■			
Carbon fixation	■					■					
Gene expression			■					■			
Generation of precursor metabolites and energy	■	■			■	■					
Glycolysis	■					■					
Nucleotide synthesis	■				■	■			■		
Pentose-phosphate pathway					■	■					
Photosynthesis	■	■	■		■	■					
Pigment biosynthesis			■							■	
Protein folding			■				■			■	
Protein modification	■					■					■
Response to toxic substance	■										
Synthesis of secondary metabolites		■	■	■					■	■	
Translation			■					■			
Specific biological processes of local infection											
Lipid modification			■		■						
Nitrogen metabolism	■		■								
Oxidation-reduction process	■										
Oxoacid metabolism	■	■	■	■	■						
Phloem development		■									
Sulphur metabolism	■		■								
Systemic acquired resistance				■							
Specific biological processes of systemic infection											
Glyoxylate and dicarboxylate metabolism						■					
Phenylpropanoid biosynthesis									■		
Protein degradation							■				
Protein export											■
RNA binding								■			

an uncharacterized protein, that was in turn co-abundant with several of these phloem proteins (Fig. 2). Why these lipoxygenases are co-abundant with phloem proteins is an interesting observation due to the need on the virus side to reach phloem. Given the lack of virus in the phloem of resistant combinations, this increase in lipoxygenases might be responding to reasons different than the mechanism of resistance itself. CmVPS41 plays a key role in cellular trafficking and membrane dynamics, which is crucial during the viral infection. The differentially accumulated PLAT-domain protein and LOXs in the resistant combinations could suggest a link between the resistant version of CmVPS41 and these proteins. Both the susceptible and the resistant versions of CmVPS41 localize to the late endosome and to the plasma membrane [31], and both play a key role in cellular trafficking and membrane dynamics, crucial during the viral infection. However, the susceptible CmVPS41 is differentially located in transvacuolar strands formed by late endosome, which are absent in the resistant genotype [31]. This differential localization in late endosome structures could trigger the differential accumulation of PLAT-domain and LOX proteins in the resistant genotypes which would not finally result in promoting viral infection.

Finally, a glycosyltransferase was uniquely up-regulated in NIL/CMV-FNY, a susceptible combination, in module 5. Glycosyltransferases are enzymes that modify oligosaccharides, proteins and lipids by adding a sugar residue, which could aid in the viral systemic infection by stabilizing viral or host proteins. For example, some glycosyltransferases have been differentially accumulated in a proteome study in *N. benthamiana*, acting as proviral factors promoting replication during *Turnip mosaic virus* infection [52]. In *Oryza sativa* (rice), glycosyltransferases are known to modify defence-related compounds, thereby influencing resistance to bacterial blight [53]. These findings provide valuable insights into the complex interactions between host proteins and CMV infection, highlighting their potential roles in plant defence and viral movement.

Systemic infection provokes increased protein degradation and phenylpropanoid biosynthesis, while decreasing translation, energy and photosynthesis

In systemic networks, we failed to map DAPs from CMV-inoculated resistant combinations, since the few DAPs observed in CMV-inoculated SC plants were not retained in the filtered network ($r=0.95$), and in the resistant CMV-LS-inoculated NIL there were no DAPs (Fig. 1C). This absence of proteomic changes aligns with previous results by [26], where the virus did not reach the systemic tissues of resistant plants. On the contrary, Fig. 3A depicts numerous perturbations in the systemic network of susceptible combinations, where NIL/CMV-FNY, PS/CMV-LS, PS/CMV-FNY presented an increase in proteins involved in protein folding, degradation, export and phenylpropanoid biosynthesis (modules 2, 5 and 6). Protein folding usually takes place at the endoplasmic reticulum (ER). However, during stress, it can also happen in other cellular compartments, where chaperones and folding factors assist in managing misfolded proteins [54] After folding, proteins enter the Golgi Apparatus and the secretory pathway, being led either to degradation in the vacuole, the PDs or to extracellular vesicles (EVs) through endosomes or Multi Vesicular Bodies (MVB) [55]. The observed changes in protein abundance related to degradation pathways may reflect the involvement of the ER-associated degradation (ERAD) pathway in CMV infection. The ERAD pathway is involved in targeting misfolded proteins for degradation at the proteasome via ubiquitination, playing an important role in protein quality control and stress responses. The Ubiquitin–proteasome degradation system (UPS) is an antiviral defence system which facilitates the targeting and degradation of viral proteins, as is the case of TMV MP, which is targeted by the 26S proteasome [55] or during *Tomato bushy stunt virus* (TBSV) infection, where a ubiquitin E3 ligase degrades the replicase, inhibiting viral replication [56]. However, the UPS system can also be exploited by viruses to favour the infection by targeting some host UPS proteins, for example, leading to disruption of defence-associated hormone signalling [57, 58]. In other cases, viruses directly use the UPS system in their life cycle. For instance, Tombusviruses use an ubiquitin-conjugating enzyme for replication as part of their replicase complex [59], while *Turnip yellow mosaic virus* (TYMV) uses ubiquitination to target its own replicase, modulating viral replication [60]. Likewise, some viral MPs are ubiquitinated and degraded by the proteasome [61], suggesting, in these cases, a role for protecting the cell from toxic over-accumulation of viral proteins. Thus, we interpret that the increased abundance of proteins related to

(See figure on next page.)

Fig. 2 Proteomic changes in local CMV infection. **A** Network of co-abundant proteins in local CMV-infected leaves. Proteins (nodes) are either circles or squares (hubs) and co-abundance is represented by edges connecting nodes. Differentially abundant proteins (DAPs) in CMV compared to mock-inoculated plants are depicted in colours. The functional characterization of each module through GO and KEGG analysis is described. Protein names of relevant proteins are depicted. 'CMVs' refer to both CMV-FNY or CMV-LS inoculated cotyledons compared to mock-inoculated ones. **B** Hubs in melon local network. Coloured cells follow the same colour code

A

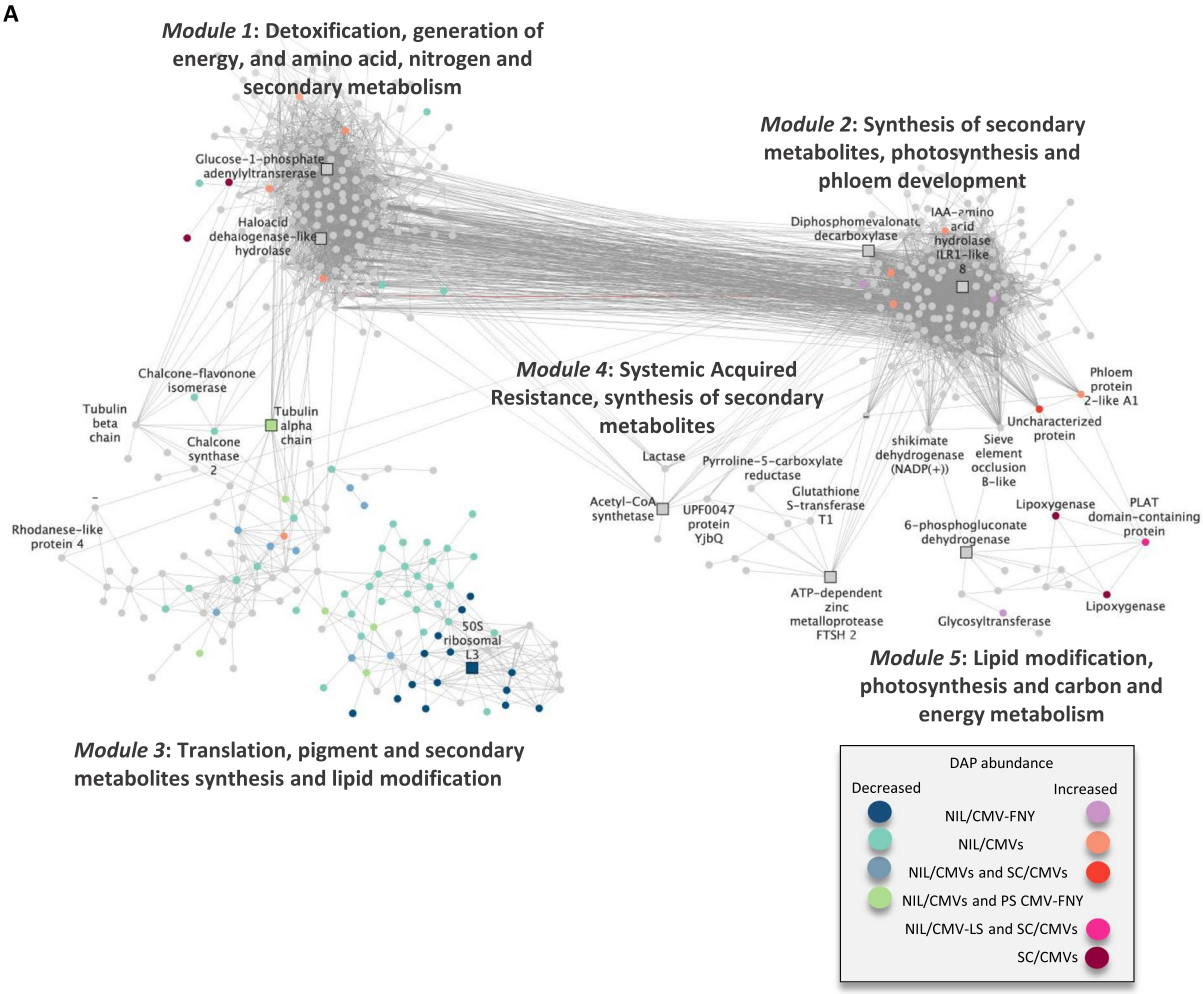

B

Hub	Name ID	Module	DAP abundance
MELO3C007747.2.1	Haloacid dehalogenase-like hydrolase	1	
MELO3C021412.2.1	Glucose-1-phosphate adenylyltransferase	1	
MELO3C005081.2.1	Diphosphomevalonate decarboxylase	2	
MELO3C018713.2.1	Acetyl-CoA synthetase	2	
MELO3C009504.2.1	Tubulin alpha chain	3	
MELO3C012357.2.1	IAA-amino acid hydrolase ILR1-like 8	3	
MELO3C022063.2.1	50S ribosomal L3	3	
MELO3C018025.2.1	ATP-dependent zinc metalloprotease FTSH 2, chloroplastic	4	
MELO3C022485.2.1	6-phosphogluconate dehydrogenase	5	

Fig. 2 (See legend on previous page.)

degradation observed in susceptible cultivars might be indicative of CMV manipulating host proteostasis via the ERAD-UPS pathway.

Additionally, DAPs increased in those susceptible combinations were related to phenylpropanoid biosynthesis, which further highlights the stress response during systemic CMV infection. Phenylpropanoids are critical in plant defence and stress responses due to their multifaceted role in strengthening plant resilience. These compounds function as antioxidants, antimicrobial agents, and structural components, playing a key role in reinforcing cell walls through the synthesis of lignin and other polymers [62, 63]. Moreover, their accumulation has been related also to virus susceptibility and symptom severity. For example, in Cucurbits, *Prunus necrotic ringspot virus* (PNRSV)-infected *Cucumis sativus* and MNSV-infected melon plants were enriched in phenylpropanoid biosynthesis enzymes, correlating in time with symptom development and severity [64]. A similar increase in phenylpropanoids was observed in *Tomato mosaic virus*-infected tomato leaves [65]. However, some studies have associated phenylpropanoids with milder symptoms or resistance [66, 67]. For example, a CMV-inoculated cucumber-resistant variety showed a threefold increase in a protein related to phenylpropanoid biosynthesis in comparison with the susceptible *C. sativus* variety [68]. Likewise, tobacco plants resistant to TMV showed an increase of phenylpropanoids upon inoculation [69], and in potato inoculated with a mild isolate from *Potato virus Y* (PVY), the mild symptomatology observed correlated with an increase in phenylpropanoids [70]. Our results support that, in the case of melon, phenylpropanoid accumulation in systemic tissues of susceptible plants, could reflect a plant response to the infection, where the plant's efforts to strengthen its defences would be overwhelmed by the virus, leading to the development of more severe symptoms, rather than limiting viral replication or movement.

The DAPs in susceptible cultivars (Fig. 3), also mapped onto communities involved in energy (module 1) and secondary metabolism and pigment synthesis (module 4). The observed decrease in these proteins indicates a disfunction of chloroplasts and photosynthetic pigments, such as chlorophyll. This is often observed during virus infections, normally leading to the disfunction of Photosystem II and the induction of viral symptoms such as mosaic and yellowing [71]. During PVY infection in tobacco plants the HCPro protease interacts with a factor involved in chloroplast division, impairing this function and leading to the depletion of chloroplast number and enlarged size in the leaves and the development of chlorotic symptoms [72]. In tobacco, TMV leads to the depletion of ferredoxin I in the chlorotic regions, where viral accumulation is increased [73]. Likewise, CMV CP interacts with ferredoxin I and disrupts its transport to the chloroplasts reducing the synthesis of chlorophyll and phytochromes and resulting in the appearance of chlorosis [74]. In fact, a similar phenomenon was observed in our network, where in module 1, a ferredoxin (Ferredoxin-NADP reductase, chloroplastic, MELO3C013765.2.1), was decreased in abundance in susceptible cultivars. Thus, our proteome data indicates that the general mosaic with chlorotic regions in infected leaves in CMV-infected systemic melon leaves was caused by the dismantling of the photosystem integrity.

Local hubs in the systemic network were explored to retrieve further central features in the viral infection. Thirteen hubs were detected across all modules, and these consistently changed across all susceptible comparisons (Fig. 3B). Among all hubs, MELO3C020563.2.1 (module 5), an ATP-dependent zinc metalloprotease Filamentation temperature-sensitive H (FTSH), decreased in abundance in CMV-inoculated plants compared to all mock-inoculated plants. FTSH proteins are critical for regulating stress responses and maintaining cellular homeostasis by ensuring protein quality [75, 76]. Decreased abundance of MELO3C020563.2.1 in CMV-inoculated plants might lead to impaired protein degradation, disrupted stress responses, and increased oxidative damage, all of which could facilitate more efficient viral replication and spread. Alternatively, these changes could also reflect the plant's own response to the viral infection, rather than direct viral effects. In this case, the reduced abundance of FTSH might indicate a plant-driven response to manage cellular stress

(See figure on next page.)

Fig. 3 Proteomic changes in systemic CMV infection. **A** Network of co-abundant proteins in systemically infected leaves. Proteins (nodes) are either circles or squares (hubs) and co-abundance is represented by edges connecting nodes. Differentially abundant proteins (DAPs) in CMV-infected compared to mock-inoculated plants are depicted in colours: red (increased abundance), blue (decreased abundance), and grey (no changes in protein abundance). The colour darkness scale indicates the presence of the same DAP in one or more pair-wise comparisons: all comparisons (darkest), 2 comparisons (medium-dark), and one comparison (lighter-shades). The functional characterization of each module through GO and KEGG analysis is described. Protein names of relevant proteins are depicted. **B** Hubs in the melon systemic network. S indicates the susceptible combinations network (PS/CMV-LS, PS/CMV-FNY and NIL/CMV-FNY comparison with their respective mock-inoculated plants); R indicates the resistant combinations network (SC/CMV-LS, SC/CMV-FNY and NIL/CMV-LS comparison with their respective mock-inoculated plants). Coloured cells follow the same colour-coded changes as in the network (A)

A

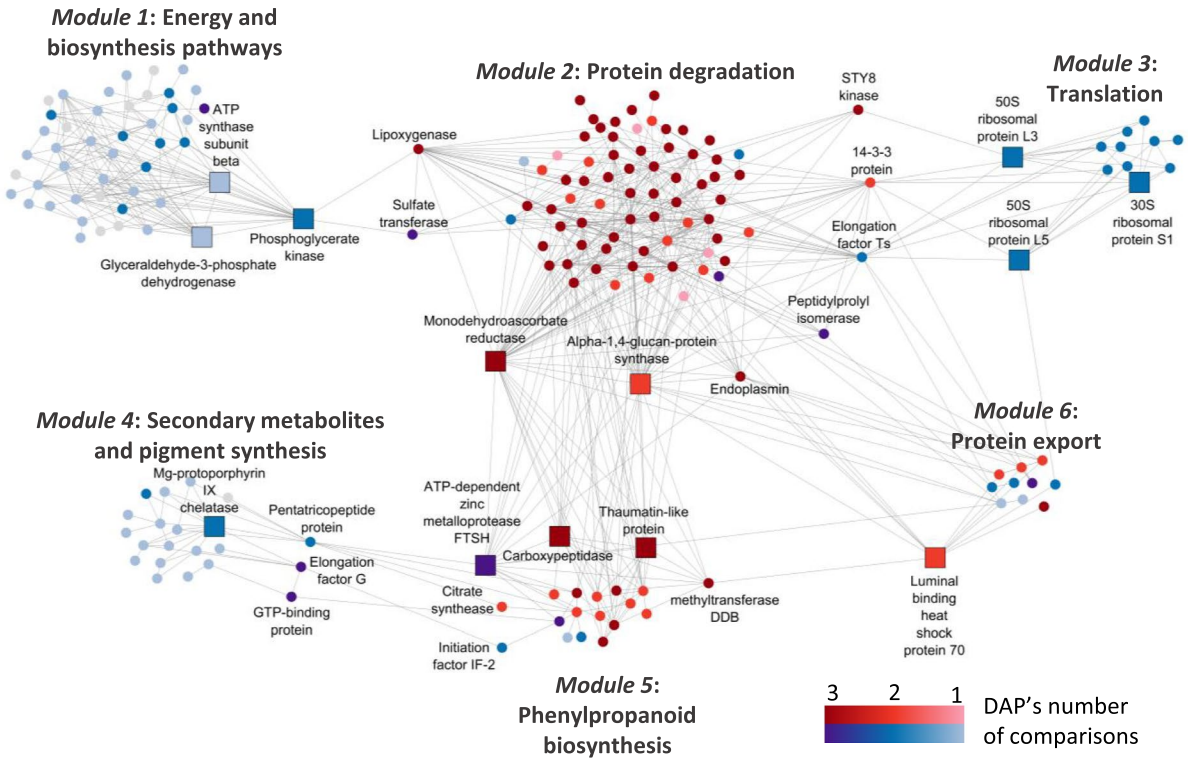

B

Hub	Name ID	Module	S	R
MELO3C019634.2.1	Phosphoglycerate kinase	1		
MELO3C017044.2.1	Glyceraldehyde-3-phosphate dehydrogenase	1		
MELO3C027174.2.1	ATP synthase subunit beta	1		
MELO3C009453.2.1	Monodehydroascorbate reductase	2		
MELO3C011416.2.1	Alpha-1,4-glucan-protein synthase	2		
MELO3C006733.2.1	30S ribosomal protein S1	3		
MELO3C006088.2.1	50S ribosomal protein L5	3		
MELO3C022485.2.1	50s ribosomal protein L3	3		
MELO3C007233.2.1	Mg-protoporphyrin IX chelatase	4		
MELO3C020563.2.1	ATP-dependent zinc metalloprotease FTSH	5		
MELO3C005643.2.1	Thaumatin-like protein	5		
MELO3C009826.2.1	Carboxypeptidase	5		
MELO3C005757.2.1	Luminal binding heat shock protein 70	6		

Fig. 3 (See legend on previous page.)

and protein quality under viral pressure, possibly aiming to conserve energy or modulate protein turnover in the face of infection. Hubs in modules 2 and 5 increased in abundance and included MELO3C009453.2.1, a monodehydroascorbate reductase involved in oxidoreductase activity [77], and MELO3C011416.2.1, an alpha-1,4-glucan-protein synthase UDP-forming, as well as MELO3C005643.2.1, a thaumatin-like protein [78], and

MELO3C009826.2.1, a carboxypeptidase involved in proteolysis [79, 80]. Both the Thaumatin-like protein and the Carboxypeptidase have been found among the altered proteins also in Nováková et al., 2020 [68] (For additional common proteins between these two studies, see Table S6). Thaumatin-like proteins (TLPs), found enriched in systemically infected susceptible plants, are associated with defence and stress responses in plants under several biotic stresses [81–83] and more specifically, seem to play a relevant role during virus infections. For example, TLPs were induced in tobacco upon TMV infection [84] and a TLP was found in a proteome of CMV-infected cucumber [68]. Furthermore, a Thaumatin-like protein was identified as an interactor of the CMV 1a protein, involved in replication, and with the MP and coat protein, both involved in the viral movement [85]. Additionally, out of the hubs in module 1, MELO3C017044.2.1, a glyceraldehyde-3-phosphate dehydrogenase (GPDH) was down-regulated in the systemic leaves of the susceptible combinations NIL/CMV-FNY and PS/CMV-LS, a trend also observed in previous studies on tomato transgenic plants resistant to CMV [86] and in cucumber plants, where GPDH was differentially accumulated in the resistant cultivar [68].

Collectively, our proteome analysis contributes to sustain that CMV infection in new leaves of susceptible cultivars induces significant proteomic changes characterized by enhanced protein abundance related to degradation pathways and phenylpropanoid biosynthesis and decreased abundance in proteins related to translation, energy and photosynthesis, indicating the readiness of the plant to deplete energy-producing pathways and enhance pathways related to defence against stress. The observed shifts in hub proteins further reveal the intricate network of responses in CMV-infected plants, highlighting the interplay between ERAD, phenylpropanoids, and the broader stress response.

Resistant and susceptible melon cultivars have protein abundance differences in local tissues but not in systemic tissues

Although heatmap analysis provided a first approach to understanding proteomic patterns between cultivars (Fig. 1A), we aimed to map differential abundance in order to more precisely compare proteome differences among genotypes. To explore this, we investigated proteomic differences in the systemic and local networks from different genotypes (PS, NIL, and SC). At cotyledons, the different cultivars showed some DAPs, whereas the new leaves of the different genotypes did not present any. As depicted in Fig. 4, in cotyledons most DAPs belong to differences between PS or NIL compared to SC and those differences in abundance were mapped in proteins that participate in the synthesis of secondary metabolites, photosynthesis and phloem development (module 2). Among the DAPs, there are two hubs that increase in abundance in module 2, a Diphosphomevalonate decarboxylase (MELO3C012357.2.1), an enzyme involved in sterol isoprenoid backbone biosynthesis, and IAA-amino acid hydrolase ILR1-like 88 (MELO3C009504.2.1), an enzyme that regulates Auxin response and thus, is involved in several developmental events in the plant. Interestingly, the three LOXs, including the PLAT-containing protein, and phloem proteins, in modules 2 and 5, were more accumulated in PS and NIL than in SC (Fig. 4). However, as shown in the CMV networks in Fig. 2, these proteins were differentially accumulated in the resistant combinations upon inoculation, suggesting that their expression could be enhanced as a response to the virus in the resistant combinations, as part of a fine-tuning of the complex molecular response during local infection. A few proteins are uniquely decreased in NIL compared to SC in module 1, involved in detoxification, metabolism, and regulatory processes. While these proteins may not be directly related to defence, their reduction in NIL but not in PS may result from interactions between the *cmv1* introgression and the PS genome, leading to subtle shifts in metabolic and regulatory pathways. Overall, DAPs common between PS and NIL compared with SC, could be due to sharing most of their genome except the introgression carrying the *cmv1* gene from SC. Instead, module 3, devoted, among others, to translation, remains mostly unchanged, indicating that most proteins are equally accumulated in all genotypes, which confirms that the general depletion of proteins in this module observed upon CMV inoculation (Fig. 2) was due to the local infection. For the complete list of DAPs between genotypes, see Table S7.

General conclusions

This study marks the first comprehensive high-throughput proteomic analysis of CMV-infected melon plants, extending beyond earlier work [33], using a more sophisticated methodology. By systems-wide network analysis we have successfully visualized and summarized integrated proteomic data, reported CMV-associated protein modules and identified key hub proteins that could serve as molecular targets for understanding and managing CMV infection. Our findings reveal distinct proteomic responses in resistant versus susceptible melon plants. In the case of local infection, resistant plants exhibit pronounced phloem-related defence mechanisms and enhanced lipid modification. In contrast, susceptible plants demonstrate broader disruptions, including decreased translation efficiency, reduced pigment and secondary metabolite synthesis,

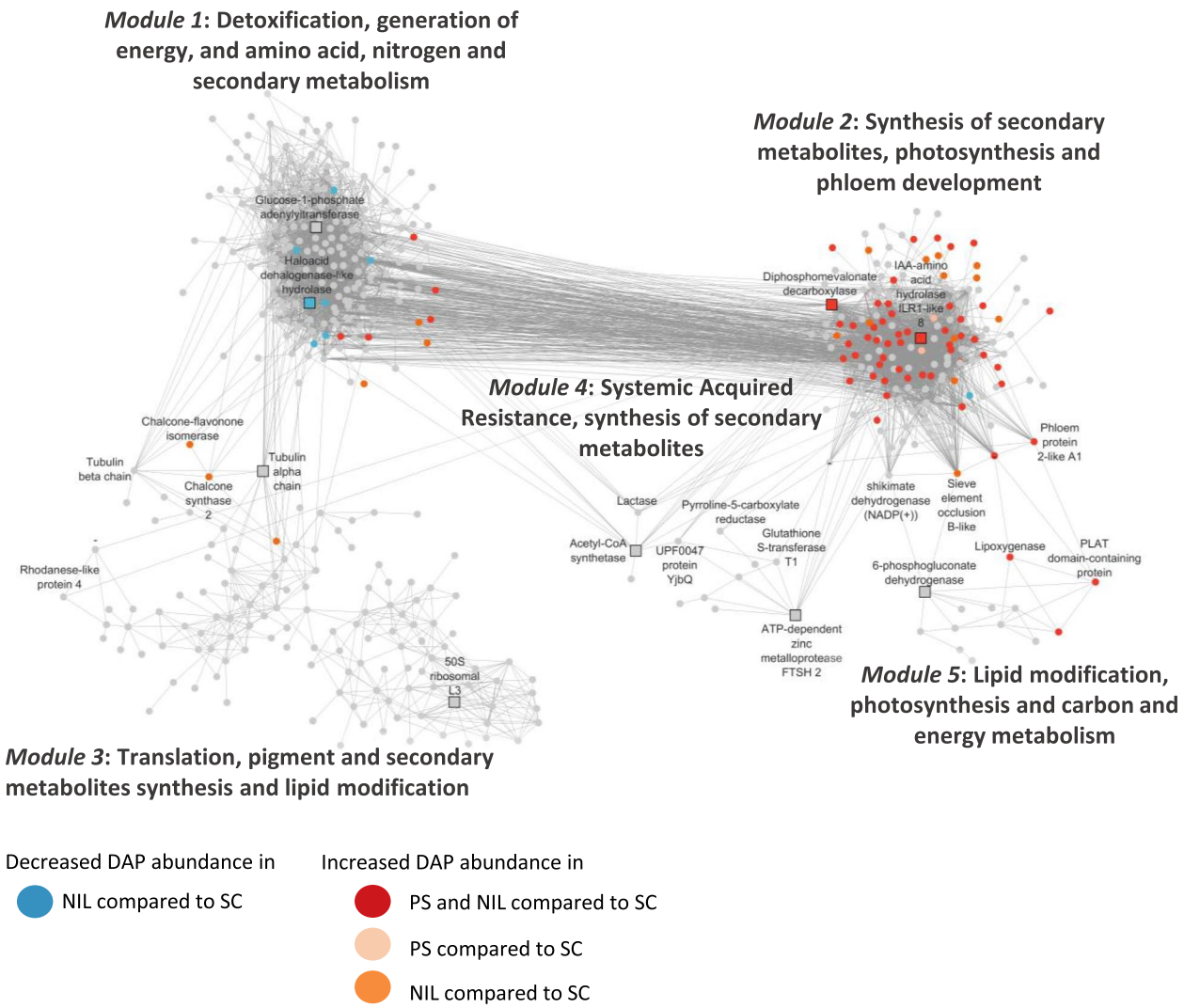

Fig. 4 Proteomic changes between cotyledons of mock-inoculated melon genotypes. Network of co-abundant proteins where proteins (nodes) are either circles or squares (hubs) and co-abundance is represented by edges connecting nodes. Differentially abundant proteins (DAPs) in one cultivar compared to another are depicted in colours. Protein names of relevant proteins are depicted

and altered lipid modifications. Later, only the systemic tissues from susceptible plants present substantial proteomic perturbations, characterized by an increased abundance of proteins involved in degradation pathways such as the ER-associated degradation (ERAD) pathway and phenylpropanoid biosynthesis, reflecting high viral replication and associated stress responses. This study provides a novel and detailed understanding of the proteomic changes associated with CMV infection, highlighting the differential responses between resistant and susceptible genotypes and identifying potential targets for future research and CMV management strategies.

Supplementary Information

The online version contains supplementary material available at https://doi.org/10.1186/s12870-025-06464-3.

Supplementary Material 1. Fig. S1. Volcano plot of NIL/CMV-FNY compared to NIL/CMV-LS in local infection.

Supplementary Material 2. Table S1. List of differentially abundant proteins (DAPs) in local infection.

Supplementary Material 3. Table S2. List of differentially abundant proteins (DAPs) in systemic infection.

Supplementary Material 4. Table S3. Number of (DAPs) in NIL12-1-99.

Supplementary Material 5. Table S4. Detailed functional annotation of co-abundant protein networks.

Supplementary Material 6. Table S5. Comparisons studied.

Supplementary Material 7. Table S6. Common proteins in systemic infection between Nováková et al, 2020 and this work.

Supplementary Material 8. Table S7. Pair-wise comparison of non-inoculated melon genotypes.

Acknowledgements
We acknowledge CRAG greenhouse service.

Authors' contributions
NR and AMM-H conceptualized the work. NR did experimental work, data analysis and wrote the original draft; AG-M contributed to data analysis and critically reviewed the manuscript; SCS helped with experimental work and data analysis; AH did experimental work. HN reviewed the manuscript and AMM-H acquired the funding, reviewed and edited the final manuscript. All authors have read and agreed to the published version of the manuscript.

Funding
This work was supported by the grants RTI2018-097665-B-C21 and PID2021-125998OB-C21, funded by MCIN/AEI/10.13039/501100011033, CEX2019-000902-S funded by MICIU/AEI/10.13039/501100011033 through the "Severo Ochoa Program for Centres of Excellence in R&D" and the CERCA Program/Generalitat de Catalunya.

Data availability
The mass spectrometry proteomics data have been deposited to the ProteomeXchange Consortium via the PRIDE [87] partner repository with the dataset identifier PXD059006.

Declarations

Ethics approval and consent to participate
The melon genotypes used were the Spanish cultivar Piel de Sapo (PS), susceptible to CMV, the Korean accession PI 161375, cultivar"Songwhan Charmi" (SC), resistant to CMV, provided by Semillas Fitó SA (Barcelona, Spain) and "La Mayora" research station (Málaga, Spain).

Consent for publication
Not applicable.

Competing interests
The authors declare no competing interests.

Author details
[1]Centre for Research in Agricultural Genomics (CRAG), CSIC-IRTA-UAB-UB, C/ Vall Moronta, Edifici CRAG, Bellaterra (Cerdanyola del Vallés), Barcelona, Spain. [2]Max Planck Institute for Plant Breeding Research, Carl-Von-Linné-Weg 10, Cologne 50829, Germany. [3]Institut de Recerca I Tecnologia Agroalimentàries (IRTA), Campus UAB, Bellaterra, Barcelona, Spain.

Received: 7 February 2025 Accepted: 25 March 2025
Published online: 05 April 2025

References

1. Csorba T, Kontra L, Burgyán J. viral silencing suppressors: tools forged to fine-tune host-pathogen coexistence. Virology. 2015;479–480:85–103.
2. Carrasco JL, Ambrós S, Gutiérrez PA, Elena SF. Adaptation of turnip mosaic virus to Arabidopsis thaliana involves rewiring of VPg-host proteome interactions. Virus Evol. 2024;10:veae055.
3. Nagy PD, Lin W. Taking over cellular energy-metabolism for TBSV replication: the high ATP requirement of an RNA virus within the viral replication organelle. Viruses. 2020;12:56.
4. Tecsi LI, Smith AM, Maule AJ, Leegood RC. A spatial analysis of physiological changes associated with infection of cotyledons of marrow plants with Cucumber mosaic virus. Plant Physiol. 1996;111:975–85.
5. Jiang T, Zhou T. Unraveling the mechanisms of virus-induced symptom development in plants. Plants. 2023;12:12.
6. Mandadi KK, Scholthof K-BG. Plant immune responses against viruses: how does a virus cause disease? Plant Cell. 2013;25:1489–505.
7. Rojas CM, Senthil-Kumar M, Tzin V, Mysore KS. Regulation of primary plant metabolism during plant-pathogen interactions and its contribution to plant defense. Front Plant Sci. 2014;5:17.
8. Culver JN, Padmanabhan MS. Virus-induced disease: altering host physiology one interaction at a time. Annu Rev Phytopathol. 2007;45:221–43.
9. Bhattacharyya D, Chakraborty S. Chloroplast: the Trojan horse in plant-virus interaction. Mol Plant Pathol. 2018;19:504–18.
10. Alexander MM, Cilia M. A molecular tug-of-war: global plant proteome changes during viral infection. Curr Plant Biol. 2016;5:13–24.
11. Kuźniak E, Kopczewski T. The chloroplast reactive oxygen species-redox system in plant immunity and disease. Front Plant Sci. 2020;11: 572686.
12. Edwardson JR, Christie RG. Cucumoviruses. In: Edwardson JR, Christie RG, editors. CRC Handbook of Viruses Infecting Legumes. Boca Raton, FL.: CRC Press; 1991. p. 293–319.
13. Palukaitis P, García-Arenal F. Cucumoviruses. Adv Virus Res. 2003;62:241–323.
14. Palukaitis P, Roossinck MJ, Dietzgen RG, Francki RI. Cucumber mosaic virus. Adv Virus Res. 1992;41:281–348.
15. Caranta C, Pflieger S, Lefebvre V, Daubèze AM, Thabuis A, Palloix A. QTLs involved in the restriction of cucumber mosaic virus (CMV) long-distance movement in pepper. Theor Appl Genet. 2002;104:586–91.
16. Ohnishi S, Echizenya I, Yoshimoto E, Boumin K, Inukai T, Masuta C. Multigenic system controlling viral systemic infection determined by the interactions between Cucumber mosaic virus genes and quantitative trait loci of soybean cultivars. Phytopathology. 2011;101:575–82.
17. Karchi Z, Cohen S, Govers A. Inheritance of resistance to cucumber mosaic virus in melons. Phytopathology. 1975;65:479–81.
18. Risser G, Pitrat M, Rode JC. Etude de la résistance du melon (Cucumis melo L.) au virus de la mosaïque du concombre. Ann Amél Plant. 1977;27:509–22.
19. Diaz JA, Mallor C, Soria C, Camero R, Garzo E, Fereres A, et al. Potential sources of resistance for melon to nonpersistently aphid-borne viruses. Plant Dis. 2003;87:960–4.
20. Pascual L, Yan J, Pujol M, Monforte AJ, Picó B, Martín-Hernández AM. CmVPS41 is a general gatekeeper for resistance to cucumber mosaic virus phloem entry in melon. Front Plant Sci. 2019;10: 1219.
21. Martín-Hernández AM, Picó B. Natural resistances to viruses in cucurbits. Agronomy. 2021;11:23.
22. Guiu-Aragonés C, Monforte AJ, Saladié M, Corrêa RX, Garcia-Mas J Martín-Hernández AM. The complex resistance to Cucumber mosaic cucumovirus (CMV) in the melon accession PI 161375 is governed by one gene and at least two quantitative trait loci. Mol Breed. 2014;34:351–62.
23. Argyris JM, Pujol M, Martín-Hernández AM, Garcia-Mas J. Combined use of genetic and genomics resources to understand virus resistance and fruit quality traits in melon. Physiol Plant. 2015;155:4–11.
24. Eduardo I, Arús P, Monforte AJ. Development of a genomic library of near isogenic lines (NILs) in melon (Cucumis melo L.) from the exotic accession PI161375. Theor Appl Genet. 2005;112:139–48.
25. Essafi A, Díaz-Pendón JA, Moriones E, Monforte AJ, Garcia-Mas J, Martín-Hernández AM. Dissection of the oligogenic resistance to Cucumber mosaic virus in the melon accession PI 161375. Theor Appl Genet. 2009;118:275–84.
26. Guiu-Aragonés C, Sánchez-Pina MA, Díaz-Pendón JA, Peña EJ, Heinlein M, Martín-Hernández AM. cmv1 is a gate for Cucumber mosaic virus transport from bundle sheath cells to phloem in melon. Mol Plant Pathol. 2016;17:973–84.
27. Guiu-Aragonés C, Díaz-Pendón JA, Martín-Hernández AM. Four sequence positions of the movement protein of Cucumber mosaic virus determine the virulence against cmv1-mediated resistance in melon. Mol Plant Pathol. 2015;16:675–84.
28. Giner A, Pascual L, Bourgeois M, Gyetvai G, Rios P, Picó B, et al. A mutation in the melon Vacuolar Protein Sorting 41prevents systemic infection of Cucumber mosaic virus. Sci Rep. 2017;7:10471.
29. Balderhaar HJK, Ungermann C. CORVET and HOPS tethering complexes - coordinators of endosome and lysosome fusion. J Cell Sci. 2013;126(Pt 6):1307–16.
30. Schoppe J, Mari M, Yavavli E, Auffarth K, Cabrera M, Walter S, et al. AP-3 vesicle uncoating occurs after HOPS-dependent vacuole tethering. EMBO J. 2020;39:e105117–e105117.

31. Real N, Villar I, Serrano I, Guiu-Aragonés C, Martín-Hernández AM. Mutations in CmVPS41 controlling resistance to cucumber mosaic virus display specific subcellular localization. Plant Physiol. 2023;191:1596–611.
32. Wang X, Li N, Li W, Gao X, Cha M, Qin L, et al. Advances in transcriptomics in the response to stress in plants. Glob Med Genet. 2020;7:30–4.
33. Malter D, Wolf S. Melon phloem-sap proteome: developmental control and response to viral infection. Protoplasma. 2011;248:217–24.
34. Serra-Soriano M, Navarro JA, Genoves A, Pallás V. Comparative proteomic analysis of melon phloem exudates in response to viral infection. J Proteomics. 2015;124:11–24.
35. Tyanova S, Temu T, Cox J. The MaxQuant computational platform for mass spectrometry-based shotgun proteomics. Nat Protoc. 2016;11:2301–19.
36. Ruggieri V, Alexiou KG, Morata J, Argyris J, Pujol M, Yano R, et al. An improved assembly and annotation of the melon (Cucumis melo L.) reference genome. Sci Rep. 2018;8:8088.
37. Lazar C, Gatto L, Ferro M, Bruley C, Burger T. Accounting for the multiple natures of missing values in label-free quantitative proteomics data sets to compare imputation strategies. J Proteome Res. 2016;15:1116–25.
38. Lazar C. imputeLCMD: a collection of methods for left-censored missing data imputation. R Packag version. 2015;2:2.
39. Shannon P, Markiel A, Ozier O, Baliga NS, Wang JT, Ramage D, et al. Cytoscape: a software environment for integrated models of biomolecular interaction networks. Genome Res. 2003;13:2498–504.
40. Clauset A, Newman MEJ, Moore C. Finding community structure in very large networks. Phys Rev E Stat Nonlin Soft Matter Phys. 2004;70(6 Pt 2):66111.
41. Kolberg L, Raudvere U, Kuzmin I, Vilo J, Peterson H. gprofiler2 – an R package for gene list functional enrichment analysis and namespace conversion toolset g:Profiler. F1000Research. 2020;9:9.
42. Giordano A, Ferriol I, López-Moya JJ, Martín-Hernández AM. cmv1-mediated resistance to CMV in melon can be overcome by mixed infections with potyviruses. Viruses. 2023;15:1792.
43. Yano R, Nonaka S, Ezura H. Melonet-DB, a grand RNA-Seq gene expression atlas in melon (Cucumis melo L.). Plant Cell Physiol. 2018;59:e4–e4.
44. Oliver S. Guilt-by-association goes global. Nature. 2000;403:601–2.
45. Wu X, Valli A, García JA, Zhou X, Cheng X. The tug-of-war between plants and viruses: great progress and many remaining questions. Viruses. 2019;11:203.
46. Boutant E, Fitterer C, Ritzenthaler C, Heinlein M. Interaction of the Tobacco mosaic virus movement protein with microtubules during the cell cycle in tobacco BY-2 cells. Protoplasma. 2009;237:3–12.
47. Trujillo DI, Silverstein KAT, Young ND. Nodule-specific PLAT domain proteins are expanded in the Medicago lineage and required for nodulation. New Phytol. 2019;222:1538–50.
48. Hyun TK, van der Graaff E, Albacete A, Eom SH, Großkinsky DK, Böhm H, et al. The Arabidopsis PLAT domain protein1 is critically involved in abiotic stress tolerance. PLoS One. 2014;9:e112946.
49. Ju L-J, Zhang C, Liao J-J, Li Y-P, Qi H-Y. An oriental melon 9-lipoxygenase gene CmLOX09 response to stresses, hormones, and signal substances. J Zhejiang Univ Sci B. 2018;19:596–609.
50. García-Marcos A, Pacheco R, Manzano A, Aguilar E, Tenllado F. Oxylipin biosynthesis genes positively regulate programmed cell death during compatible infections with the synergistic pair potato virus X-potato virus Y and Tomato spotted wilt virus. J Virol. 2013;87:5769–83.
51. Song H, Wang P, Li C, Han S, Lopez-Baltazar J, Zhang X, et al. Identification of lipoxygenase (LOX) genes from legumes and their responses in wild type and cultivated peanut upon *Aspergillus flavus* infection. Sci Rep. 2016;6:35245.
52. Ding K, Jia Z, Rui P, Fang X, Zheng H, Chen J, et al. Proteomics identified UDP-Glycosyltransferase family members as pro-viral factors for turnip mosaic virus infection in nicotiana benthamiana. Viruses. 2023;15:15.
53. Lin Y, Lian L, Zhu Y, Wang L, Li H, Zheng Y, et al. Characterization and expression analysis of the glycosyltransferase 64 family in rice (*Oryza sativa*). Gene. 2022;838: 146708.
54. Pulido P, Zagari N, Manavski N, Gawronski P, Matthes A, Scharff LB, et al. Chloroplast ribosome associated supports translation under stress and interacts with the ribosomal 30S subunit. Plant Physiol. 2018;177:1539–54.
55. Reichel C, Beachy RN. Degradation of tobacco mosaic virus movement protein by the 26S proteasome. J Virol. 2000;74:3330–7.
56. Barajas D, Kovalev N, Qin J, Nagy PD. Novel mechanism of regulation of tomato bushy stunt virus replication by cellular WW-domain proteins. J Virol. 2015;89:2064–79.
57. Jia Q, Liu N, Xie K, Dai Y, Han S, Zhao X, et al. CLCuMuB βC1 subverts ubiquitination by interacting with NbSKP1s to enhance geminivirus infection in *Nicotiana benthamiana*. PLoS Pathog. 2016;12: e1005668.
58. Liu S, Wang C, Liu X, Navas-Castillo J, Zang L, Fan Z, et al. Tomato chlorosis virus-encoded p22 suppresses auxin signalling to promote infection via interference with SKP1-Cullin-F-box(TIR1) complex assembly. Plant Cell Environ. 2021;44:3155–72.
59. Imura Y, Molho M, Chuang C, Nagy PD. Cellular Ubc2/Rad6 E2 ubiquitin-conjugating enzyme facilitates tombusvirus replication in yeast and plants. Virology. 2015;484:265–75.
60. Camborde L, Planchais S, Tournier V, Jakubiec A, Drugeon G, Lacassagne E, et al. The ubiquitin-proteasome system regulates the accumulation of Turnip yellow mosaic virus RNA-dependent RNA polymerase during viral infection. Plant Cell. 2010;22:3142–52.
61. Niehl A, Amari K, Gereige D, Brandner K, Mély Y, Heinlein M. Control of tobacco mosaic virus movement protein fate by CELL-DIVISION-CYCLE Protein48. Plant Physiol. 2012;160:2093–108.
62. Ortiz A, Sansinenea E. Phenylpropanoid derivatives and their role in plants' health and as antimicrobials. Curr Microbiol. 2023;80:380.
63. Naoumkina MA, Zhao Q, Gallego-Giraldo L, Dai X, Zhao PX, Dixon RA. Genome-wide analysis of phenylpropanoid defence pathways. Mol Plant Pathol. 2010;11:829–46.
64. Bellés JM, López-Gresa MP, Fayos J, Pallás V, Rodrigo I, Conejero V. Induction of cinnamate 4-hydroxylase and phenylpropanoids in virus-infected cucumber and melon plants. Plant Sci. 2008;174:524–33.
65. López-Gresa MP, Lisón P, Kim HK, Choi YH, Verpoorte R, Rodrigo I, et al. Metabolic fingerprinting of tomato mosaic virus infected *Solanum lycopersicum*. J Plant Physiol. 2012;169:1586–96.
66. Kandan A, Commare RR, Nandakumar R, Ramiah M, Raguchander T, Samiyappan R. Induction of phenylpropanoid metabolism byPseudomonas fluorescens against tomato spotted wilt virus in tomato. Folia Microbiol (Praha). 2002;47:121–9.
67. Shadle GL, Wesley SV, Korth KL, Chen F, Lamb C, Dixon RA. Phenylpropanoid compounds and disease resistance in transgenic tobacco with altered expression of l-phenylalanine ammonia-lyase. Phytochemistry. 2003;64:153–61.
68. Nováková S, Šubr Z, Kováč A, Fialová I, Beke G, Danchenko M. Cucumber mosaic virus resistance: Comparative proteomics of contrasting Cucumis sativus cultivars after long-term infection. J Proteomics. 2020;214: 103626.
69. Choi YH, Kim HK, Linthorst HJM, Hollander JG, Lefeber AWM, Erkelens C, et al. NMR metabolomics to revisit the tobacco mosaic virus infection in *Nicotiana tabacum* Leaves. J Nat Prod. 2006;69:742–8.
70. Kogovšek P, Pompe-Novak M, Petek M, Fragner L, Weckwerth W, Gruden K. Primary metabolism, phenylpropanoids and antioxidant pathways are regulated in potato as a response to potato virus Y infection. PLoS One. 2016;11: e0146135.
71. Lehto K, Tikkanen M, Hiriart J-B, Paakkarinen V, Aro E-M. Depletion of the photosystem II core complex in mature tobacco leaves infected by the flavum strain of tobacco mosaic virus. Mol Plant Microbe Interact. 2003;16:1135–44.
72. Tu Y, Jin Y, Ma D, Li H, Zhang Z, Dong J, et al. Interaction between PVY HC-Pro and the NtCF1β-subunit reduces the amount of chloroplast ATP synthase in virus-infected tobacco. Sci Rep. 2015;5:15605.
73. Ma Y, Zhou T, Hong Y, Fan Z, Li H. Decreased level of ferredoxin I in Tobacco mosaic virus-infected tobacco is associated with development of the mosaic symptom. Physiol Mol Plant Pathol. 2008;72:39–45.
74. Song XS, Wang YJ, Mao WH, Shi K, Zhou YH, Nogués S, et al. Effects of cucumber mosaic virus infection on electron transport and antioxidant system in chloroplasts and mitochondria of cucumber and tomato leaves. Physiol Plant. 2009;135:246–57.
75. Yi L, Liu B, Nixon PJ, Yu J, Chen F. Recent advances in understanding the structural and functional evolution of FtsH proteases. Front Plant Sci. 2022;13: 837528.
76. Krynická V, Komenda J. The role of FtsH complexes in the response to abiotic stress in cyanobacteria. Plant Cell Physiol. 2024;65:1103–14.
77. Fukao Y, Ferjani A, Fujiwara M, Nishimori Y, Ohtsu I. Identification of zinc-responsive proteins in the roots of Arabidopsis thaliana using a highly

improved method of two-dimensional electrophoresis. Plant Cell Physiol. 2009;50:2234–9.
78. Capelli N, Diogon T, Greppin H, Simon P. Isolation and characterization of a cDNA clone encoding an osmotin-like protein from *Arabidopsis thaliana*. Gene. 1997;191:51–6.
79. Bayer EM, Bottrill AR, Walshaw J, Vigouroux M, Naldrett MJ, Thomas CL, et al. Arabidopsis cell wall proteome defined using multidimensional protein identification technology. Proteomics. 2006;6:301–11.
80. Aryal UK, Xiong Y, McBride Z, Kihara D, Xie J, Hall MC, et al. A proteomic strategy for global analysis of plant protein complexes. Plant Cell. 2014;26:3867–82.
81. Mahdavi F, Sariah M, Maziah M. Expression of rice thaumatin-like protein gene in transgenic banana plants enhances resistance to fusarium wilt. Appl Biochem Biotechnol. 2012;166:1008–19.
82. de Jesús-Pires C, Ferreira-Neto JRC, Pacifico Bezerra-Neto J, Kido EA, de Oliveira Silva RL, Pandolfi V, et al. Plant thaumatin-like proteins: function, evolution and biotechnological applications. Curr Protein Pept Sci. 2020;21:36–51.
83. Zhang Y, Chen W, Sang X, Wang T, Gong H, Zhao Y, et al. Genome-wide identification of the thaumatin-like protein family genes in gossypium barbadense and analysis of their responses to verticillium dahliae infection. Plants (Basel, Switzerland). 2021;10:2647.
84. Albrecht H, van de Rhee MD, Bol JF. Analysis of cis-regulatory elements involved in induction of a tobacco PR-5 gene by virus infection. Plant Mol Biol. 1992;18:155–8.
85. Kim MJ, Ham B-K, Kim HR, Lee I-J, Kim YJ, Ryu KH, et al. In vitro and in planta interaction evidence between *Nicotiana tabacum* thaumatin-like protein 1 (TLP1) and cucumber mosaic virus proteins. Plant Mol Biol. 2005;59:981–94.
86. Di Carli M, Villani ME, Bianco L, Lombardi R, Perrotta G, Benvenuto E, et al. Proteomic analysis of the plant-virus interaction in cucumber mosaic virus (CMV) resistant transgenic tomato. J Proteome Res. 2010;9:5684–97.
87. Perez-Riverol Y, Bandla C, Kundu DJ, Kamatchinathan S, Bai J, Hewapathirana S, et al. The PRIDE database at 20 years: 2025 update. Nucleic Acids Res. 2025;53:D543–53.

Publisher's Note